

Research



Cite this article: Taffet EJ, Fassioli F, Toa ZSD, Beljonne D, Scholes GD. 2020 Uncovering dark multichromophoric states in Peridinin–Chlorophyll–Protein. *J. R. Soc. Interface* **17**: 20190736.
<http://dx.doi.org/10.1098/rsif.2019.0736>

Received: 28 October 2019

Accepted: 28 February 2020

Subject Category:

Life Sciences–Chemistry interface

Subject Areas:

biophysics

Keywords:

excitons, charge-transfer, correlated triplet pair

Author for correspondence:

Elliot J. Taffet

e-mail: etaffet@princeton.edu

Electronic supplementary material is available online at <https://doi.org/10.6084/m9.figshare.c.4881015>.

Uncovering dark multichromophoric states in Peridinin–Chlorophyll–Protein

Elliot J. Taffet^{1,2}, Francesca Fassioli^{1,3}, Zi S. D. Toa¹, David Beljonne² and Gregory D. Scholes¹

¹Department of Chemistry, Princeton University, Washington Road, Princeton, NJ 08540, USA

²Department of Chemistry, University of Mons, 7000 Mons, Belgium

³SISSA – Scuola Internazionale Superiore di Studi Avanzati, Trieste, Italy

EJT, 0000-0002-8321-5116; ZSDT, 0000-0003-2890-6579

It has long been recognized that visible light harvesting in Peridinin–Chlorophyll–Protein is driven by the interplay between the bright (S_2) and dark (S_1) states of peridinin (carotenoid), along with the lowest-lying bright (Q_y) and dark (Q_x) states of chlorophyll-*a*. Here, we analyse a chromophore cluster in the crystal structure of Peridinin–Chlorophyll–Protein, in particular, a peridinin–peridinin and a peridinin–chlorophyll-*a* dimer, and present quantum chemical evidence for excited states that exist beyond the confines of single peridinin and chlorophyll chromophores. These dark multichromophoric states, emanating from the intermolecular packing native to Peridinin–Chlorophyll–Protein, include a correlated triplet pair comprising neighbouring peridinin excitations and a charge-transfer interaction between peridinin and the adjacent chlorophyll-*a*. We surmise that such dark multichromophoric states may explain two spectral mysteries in light-harvesting pigments: the sub-200-fs singlet fission observed in carotenoid aggregates, and the sub-200-fs chlorophyll-*a* hole generation in Peridinin–Chlorophyll–Protein.

1. Introduction

Photosynthesis is made possible by intricate biological pigment–protein complexes that trap energy from the sun and subsequently transfer electronic excitation energy so as to spur charge separation in the reaction centre [1]. Nature's interchromophore orientation in these complexes may have underlying significance for engendering efficient energy transfer crucial to the light-harvesting mechanism [2]. This energy transfer arises from the interplay between polyene-like carotenoids (Cars) surrounding porphyrin-like (bacterio)chlorophyll (Chl) chromophores [1,3]. Achieving effective interplay is especially important in Peridinin–Chlorophyll–Protein (PCP) found in dinoflagellates [3]. Dinoflagellates are positioned in the water column in such a way that the most abundant source of (limited) light energy available to them is in the 450–550 nm range where Cars uniquely absorb—meaning PCP light harvesting is driven by peridinin Cars [4], in stark contrast to most other membrane-bound photosynthetic antennae that experience (bacterio)Chl-driven light harvesting. Cars in PCP surround neighbouring Chl-*a* in a 4:1 Car:Chl stoichiometric ratio [3]. Each cluster of closely packed chromophores in PCP has precisely four Car and one Chl, with two such clusters comprising a PCP protein subunit, of which there are three in an overall trimeric complex as identified from the crystal structure of the dinoflagellate *Amphidinium carterae* [3,5]. As the trimeric PCP simply is the combination of identical chromophore cluster pairs forming individual subunits, it seems reasonable to deduce that the chromophore interaction within these clusters forms the basis for energy transfer [3].

As energy transfer results from 450 to 550 nm absorbed solar energy donated exclusively by Cars to accepting Chl, researchers have focused on the intrinsic manifold of Car and Chl excited states to describe this process [1,3]. Car excited states involved in light harvesting may be traced back to those of their parent

polyene backbones, while the corresponding Chl excited states stem from quasi-orthogonal polarization directions in the plane of its porphyrin ring [6]. Since the foundational discovery by Hudson & Kohler nearly 50 years ago of anomalous fluorescence in a functionalized polyene [7], carotenoids have been described as exhibiting a lowest-lying dark one-photon-forbidden excited state labelled S_1 . This labelling casts the dark state as being energetically below the bright one-photon-allowed excited state labelled S_2 [4].

It should be mentioned, however, that while the dark S_1 state has been identified from experimental fluorescence spectroscopy [8,9], additional dark states of possibly intermediate excitation energy between S_2 and S_1 have been proposed [10], but have not been straightforwardly identified—thereby remaining controversial assignments [4,11]. On the other hand, the assignment of the two lowest-lying states of Chl-*a*, the dark Q_x and the bright Q_y in the quasidegenerate Q band, dates back to the early 1960s [12,13], and this nomenclature remains in use today [4]. In this case, the only lingering question concerns the relative energetic position of the dark Q_x state, which cannot clearly be distinguished from the vibronic progression of the bright Q_y state in experimental absorption spectroscopy [12,14–17].

Might Car–Chl energy transfer in PCP stem simply from the basis of these four identified individual-chromophore excited states, two on each chromophore? The exceptional energy-transfer efficiency of PCP suggests otherwise [3]. While the S_2 and S_1 emission spectra generally overlap well with the corresponding Q_x and Q_y absorption spectra, energy transfer from the bright S_2 state [18]—more strongly coupled than S_1 to Chl-*a* states through its large transition dipole [3]—needs to compete with ultrafast Car S_2 – S_1 internal conversion in the time scale of 50–300 fs [19]. Internal conversion could entail significant efficiency losses in energy transfer.

Nonetheless, this framework ignores the unique chemical nature of the peridinin Car—containing an allene tail and a lactone ring—that may support intramolecular-charge-transfer (ICT) character and even a separate ICT state [20]. Yet much like the claims of spectral evidence for dark intermediate states, the nature of ICT in peridinin remains controversially assigned, as evidenced by twenty-first-century experimental [21–23] and computational [24–27] investigations. On one hand, red-shifted emission with diminished lifetime in the face of polar solvent [20] and a distinct low-lying electronic excited state with ICT character [24] have been reported; on the other hand, conformational bright-state local minima [21,22] and bond-vibration-driven interplay between the lowest-lying bright- and dark-state properties [25] have been proposed as explanations for peridinin’s anomalous photophysics. Whether ICT character exists as its own independent electronic excited state, and whether it impacts S_2/S_1 state properties, may have important implications in energy transfer. Imbuing the lowest-lying state with bright-state-like properties through ICT character may well represent the key missing ingredient explaining the energy-transfer efficiency in PCP [3,28].

But what about the impact of intermolecular interaction on the manifold of Car and Chl states? This computationally under-explored question touches on the role of the biological supramolecular organization in mediating Car and Chl photosynthetic function. It is well known that electronic coupling may give rise to exciton migration among delocalized excited states [29]. Exciton theory describes this delocalization by including

the coupling matrix elements between diabatic states expressed in the basis of individual chromophores [30,31]. This leads to a coherent superposition of localized molecular states that coherently spreads the excitation across the molecular network.

While pigment–protein complexes have been described as ‘warm, wet and noisy’ [32], intimating that incoherent dynamics in response to light dominate, others have argued for the existence of an underlying order in the supramolecular assembly in which the structure of the molecular environment may also support quantum coherent *dynamical* effects [2,29–43]. Here, we investigate *static* effects in the context of dark states distributed across dimers.

In this report, we present quantum chemical calculations supplying evidence for dark multichromophoric excited states that are indescribable in single-chromophore bases. Unlike the physical picture in exciton theory, in which coupling delocalizes the excited state by creating a superposition of locally excited (LE) states, these dark multichromophoric states are *inherently* non-local. A Car dimer system seems to support a correlated triplet pair state in which local Car-specific triplet excitations are coupled into an overall spin singlet state. On the other hand, a Car–Chl dimer system seems to support the *intermolecular* charge-transfer character in which the excited electron on the Car comes from the Chl-*a* chromophore. On the basis of their excitation energies, we surmise that these dark multichromophoric states may unlock alternative pathways to visible light harvesting in PCP. These include sub-200-fs singlet fission observed previously in carotenoid aggregates [44] and sub-200-fs ground-state bleaching of Chl-*a* stemming from hole generation following Car optical excitation in ultrafast laser spectroscopy [3,27,28]. We also present quantum chemical evidence for direct peridinin S_2 – S_1 internal conversion in the single-molecule picture without the involvement of intermediate states—ICT or otherwise—with S_1 falling below the photoexcited-state energy following nuclear reorganization as we, and others, have previously found [25,45,46]. The lowest-lying Car bright and dark states are shown to be quasidegenerate prior to S_1 population. We, therefore, dispense with the term ‘intermediate’ when describing our calculated dark multichromophoric states.

In this paper, we compute excited-state manifolds—both intramolecular and intermolecular—corresponding to the chromophore cluster containing peridinin residues 611N and 612N along with the adjacent Chl-*a* residue 601N. We preserve the intramolecular conformations and intermolecular orientations of these residues in the PCP crystal structure. We refer the reader to our earlier work [47] detailing the theoretical treatment applied here to investigate energetically relevant dark multichromophoric excited states so as to comment on their potential roles in the light-harvesting mechanism of PCP.

2. 611N crystal-structure results

Let us first consider the individual peridinin residue 611N so as to ground ourselves in the intrinsic peridinin photophysical framework within PCP. Our results suggest that neither in the ground-state biological conformation—assumed to be statically represented by the crystal-structure geometry—nor in the relaxed excited-state equilibria does an intermediate excited state between S_1 and S_2 manifest.

Our results stem from the application of multireference state-averaged complete-active-space self-consistent field

Table 1. The low-lying electronic excited states of peridinin 611N at its crystal-structure geometry (transition dipole moment in Debye, excitation energy in eV, N_{odd} = odd-electron count defined in equation (3.1)).

state	excitation energy	active space	transition dipole moment	predominant configuration	N_{odd}	assignment
S_1	2.12	(16,16)	0.238	HOMO ² LUMO ²	3.03	dark
S_2	2.24	(4,4)	16.1	HOMO LUMO	2.09	bright
S_3	3.02	(16,16)	0.552	HOMO LUMO HOMO-1 LUMO		dark
S_4	3.76	(16,16)	0.660	HOMO-1 LUMO HOMO-1 LUMO		dark
S_5	4.17	(16,16)				dark
S_6	4.49	(16,16)				dark
S_7	4.76	(16,16)				dark

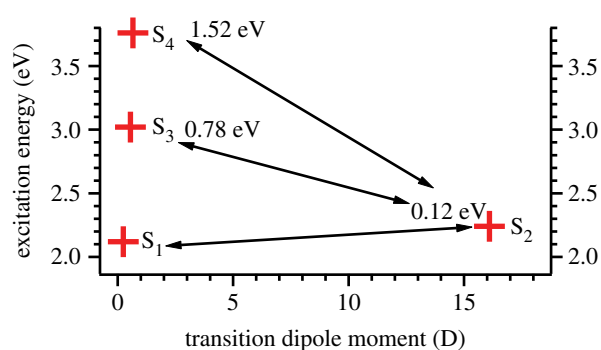


Figure 1. The excitation energies of the four lowest-lying excited states of peridinin with respect to their oscillator strengths. Arrows are for visualization of the excitation-energy difference between each dark state (S_1 , S_3 and S_4) and the bright state (S_2), which is labelled next to the higher-lying state. The dark S_1 , S_3 and S_4 states are clearly distinguishable from the bright S_2 state in terms of their transition dipole moments.

(CASSCF) and its approximate density-matrix-renormalization-group (DMRGSCF) form paired with second-order N -electron valence-state perturbation theory (NEVPT2)—an approach we have applied previously [45,47,48]—to capture the different electron-correlation types defining bright and dark states. Our optimal results from the best variational wave functions, tabulated in table 1 and graphically displayed in figure 1 for different active spaces, suggest that the S_1 and S_2 states are quasidegenerate for 611N in its crystal structure. Moreover, the peridinin 611N S_1 and S_2 states appear polyene-like in their character—the S_1 dark state features a lower transition dipole moment by over an order of magnitude (table 1). Just as important as this distinction is the lack of distinguishable ICT character in the excited states. Though it is not clearly attributable to a conformational effect from Nature's interchromophore packing rather than uncertainty in the crystal-structure bond lengths, this result

suggests S_1 population may be mediated by near-degeneracy with S_2 (table 1 and figure 1).

3. 611N crystal-structure discussion

Given that the S_1 state is below the S_2 state by only 0.12 eV in the crystal-structure geometry of peridinin 611N, it would seem that these two states would be able to couple directly through off-diagonal elements of the nuclear kinetic energy operator—vibronic coupling—without a bridging intermediate state. S_1 and S_2 appear traceable to the dark and bright states of polyenes based on their predominant wave function configurations as we previously noted [45].

Yet it must be noted that the dark S_1 state is not a pure correlated triplet pair as it historically has been rationalized to be [49,50]. This is suggested by the calculated odd-electron count (N_{odd}) displayed in table 1, which is defined by the following equation [51]:

$$N_{\text{odd}} = 2(\text{Tr}[\gamma] - \text{Tr}[\gamma\gamma^+]) = 2(N - \text{Tr}[\gamma\gamma^+]), \quad (3.1)$$

where γ corresponds to the state's one-particle density matrix. The number is equivalent to four for a pure correlated triplet pair of non-interacting triplet excitations, since the individual triplets would consist of two unpaired electrons each. The near-integer deviation from this ideal value indicates that the intrinsic peridinin S_1 state is an impure dark correlated triplet pair—one that, due to this impurity, lacks the wave function character to split into two triplets (singlet fission).

The interplay between the S_2 and S_1 states is mediated by non-symmetric vibrational modes according to their idealized respective B_u and A_g state irreducible representations in group theory. As these non-symmetric modes are Franck–Condon inactive, intramolecular vibrational redistribution (IVR) must preface population transfer from S_2 to S_1 , and IVR may manifest in the 50–300-fs lifetime of the peridinin S_2 state [3].

Table 2. Manifold of peridinin excited states at its relaxed S_2 equilibrium geometry following reorganization in a frozen MM environment of surrounding PCP molecular residues (transition dipole moment in Debye, excitation energy in eV, N_{odd} = odd-electron count defined in equation (3.1)).

state	excitation energy	active space	transition dipole moment	predominant configuration	N_{odd}	assignment
S_1	2.68	(16,16)	0.446	HOMO ² LUMO ²	2.53	dark
S_2	2.58	(4,4)	14.6	HOMO LUMO	2.03	bright
S_3	3.58	(16,16)	0.223	HOMO LUMO HOMO-1 LUMO		dark
S_4	4.37	(16,16)	0.145	(HOMO-1) ² LUMO ²		dark

4. 611N equilibrium-structure results

The interplay between S_1 and S_2 is further evidenced by an energetic inversion between still-quasidegenerate S_2 and S_1 , stemming from nuclear reorganization in the peridinin 611N S_2 state. We consider this nuclear reorganization in the PCP environment by calculating the peridinin 611N S_2 (QM, TDA) equilibrium geometry in the presence of all surrounding amino acids and lipids in subunit N, as well as the surrounding three Car and one Chl-*a* in the half-subunit chromophore cluster (Computational details). Our results, tabulated in table 2 and graphically displayed in figure 2, suggest that this reorganization serves to drive peridinin closer to its minimum ground-state potential away from the more displaced crystal-structure geometry. As a result of the relatively flat S_2 potential, the effect of this reorganization is to raise the S_0 - S_2 excitation energy but more significantly increase that of S_0 - S_1 (table 2 and figure 2).

The counter-intuitive nuclear reorganization in S_2 from the crystal structure—a highly distorted peridinin conformation—involves C=C contraction rather than elongation as we have reported previously for polyenes [47] and for peridinin [45] from an S_0 equilibrium geometry. Owing to intrinsic uncertainty in the protein crystal structure, it is unclear as to whether the geometric distortions in the 611N crystal-structure geometry are consequences of biological orientation or artefacts of extracting nuclear coordinates from a crystal structure.

Nonetheless, within the domain of the computational chemistry applied (Computational details), it is apparent that excited-state nuclear reorganization in S_1 under the same QM/MM framework breaks the quasidegeneracy computed for the S_2 equilibrium. Using CASSCF to describe the dark S_1 state electronic structure, we find that S_1 stabilizes through C=C bond-length elongation back toward crystal-structure values and away from the S_2 equilibrium values. Therefore, this reorganization has the effect of re-introducing the conventional ordering of states— S_1 below S_2 —that appears in the quasidegenerate manifold corresponding to the crystal structure (table 3 and figure 2).

5. Intermolecular dimer-pair results

Now let us switch to the multichromophoric picture by considering how intermolecular interactions between peridinin 611N

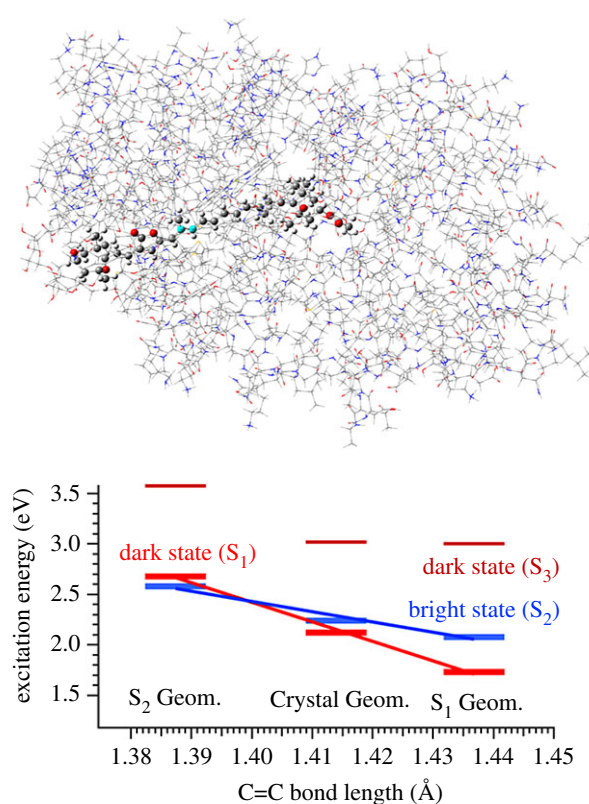


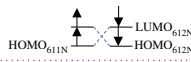
Figure 2. Summary of nuclear reorganization from the crystal structure in the S_2 and S_1 states. Peridinin 611N (ball-and-stick representation) reorganizes in S_2 through C=C bond-length contraction, whereas it reorganizes in S_1 through C=C bond-length elongation relative to the crystal-structure geometry (Geom.). S_1 and S_2 excitation energies are shown to decrease with increased C=C bond-length elongation, but the S_1 state is more strongly stabilized by this distortion on account of the greater displacement of its minimum from the S_0 equilibrium geometry.

and its neighbouring 612N peridinin residue, along with its neighbouring 601N Chl-*a* residue, impact the manifold of states. Here, we separately analyse the intermolecular Car-Car dimer 611N-612N system and the intermolecular Car-Chl 611N-601N pair using DMRGSCF quantum chemistry paired with NEVPT2. We compute two additional low-lying excited states that do not appear in the intrinsic peridinin 611N or Chl-*a* 601N manifold—diagnosing them as dark

Table 3. Manifold of peridinin excited states at its relaxed S_1 equilibrium geometry following reorganization in a frozen MM environment of surrounding PCP molecular residues (transition dipole moment in Debye, excitation energy in eV, N_{odd} = odd-electron count defined in equation (3.1)).

state	excitation energy	active space	transition dipole moment	predominant configuration	N_{odd}	assignment
S_1	1.73	(16,16)	0.194	HOMO ² LUMO ²	3.21	dark
S_2	2.08	(4,4)	15.2	HOMO LUMO	2.15	bright
S_3	3.00	(16,16)	0.700	HOMO-2 LUMO		dark
S_4	3.83	(16,16)	0.113	HOMO-3 LUMO		dark

Table 4. Manifold of 611N–612N intermolecular peridinin dimer and 611N–601N Car–Chl pair states (excitation energies relevant to energy transfer bolded, transition dipole moment in Debye, excitation energy in eV, N_{odd} = odd-electron count defined in equation (3.1)).

state	excitation energy	excitation type	active space	transition dipole moment	predominant configuration	N_{odd}	assignment
Q_y	1.75	absorption	(8,8)	9.29	HOMO _{Chl-a} LUMO _{Chl-a}		bright
S_1	2.65	absorption	(8,8)	0.483	HOMO _{Car} ² LUMO _{Car} ²		dark
S_1	1.73	emission	(16,16)	0.328	HOMO _{Car} ² LUMO _{Car} ²	3.21	dark
Q_x	3.03	absorption	(8,8)	1.55	HOMO-1 _{Chl-a} LUMO _{Chl-a}		dark
S^*	2.11	absorption	(8,8)	2.39×10^{-4}		4.00	dark
CT	2.58	absorption	(8,8)	9.06×10^{-4}	HOMO _{Chl-a} LUMO _{Car}		dark
$T_1 + T_2$	2.10	absorption	(8,8)				

multichromophoric states. As summarized in table 4 and figure 3, these states, which we call S^* and CT (not the intramolecular CT state intrinsic to peridinin [24], but rather a dimeric CT that appear in the respective Car–Car and Car–Chl systems (*vide infra*), open up alternative pathways to intrinsic S_2 – S_1 Car internal conversion by spreading electronic excitation energy across multiple chromophores.

6. Intermolecular dimer-pair discussion

6.1. The Car–Chl 611N–601N dimer

In table 4, we list the intrinsic Chl- a Q_x and Q_y states identified from computation on the Car–Chl pair system. The Chl- a Q_y state wave function has been reported to consist of a predominantly Chl- a HOMO–LUMO transition, while that for Q_x a HOMO–LUMO+1 transition [52], and we recover corresponding excited states with these predominant configurations in our calculations. We similarly distinguish the

Car S_1 state within the Car–Chl manifold based on its retained predominant double-excitation configuration.

With the Car- and Chl-specific excited states identified within the multichromophoric picture, we note that an additional singlet excited state appears in our five-singlet-state-averaged calculation. This state is computed to have a predominant HOMO–LUMO transition in the multichromophoric system—that is, the state comprises an excitation from the Chl- a HOMO to the Car LUMO. This makes such a dark multichromophoric state a CT excitation. The CT state is supported by through-space electrostatic interactions between the confined Car and Chl- a chromophores within the PCP chromophore cluster. Owing to the long-range intermolecular electron-hole separation associated with this state, it attains an exceptionally dark character—a transition dipole moment over four orders of magnitude below that of the bright Car state! Therefore, its identification would prove exceptionally challenging in steady-state experimental spectroscopy, given that the oscillator strength is so far below those of the intrinsic putative ‘dark’ excited states of Car and Chl- a : S_1 and Q_x . The CT state excitation

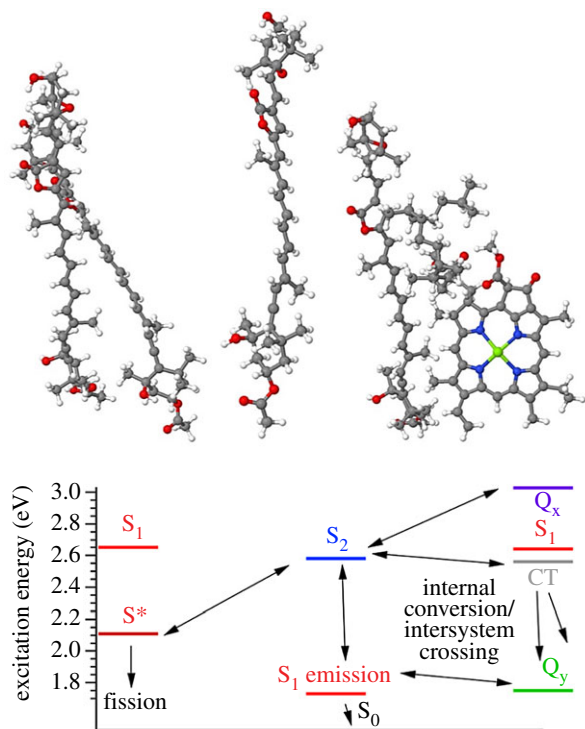


Figure 3. Excitation energies of all excited states of interest—intrinsic to peridinin and multichromophoric—as well as the possible pathways connecting them. The anticipated interplay between computed excited states is denoted by double-headed arrows, while the fates of these excited states are denoted by single-headed arrows. On either side of the intrinsic peridinin S_1 and S_2 states (emission energies shown), we display the intrinsic Chl- a Q_y and Q_x states, as well as the S^* and CT dark multichromophoric states next to the identified S_1 computed for these systems.

energy of 2.58 eV is robust to active-space expansion (changing by only 0.06 eV following a larger 16-orbital-active-space calculation) and is, therefore, proximal to the computed S_2 emission energy. Yet it is assumed here that biological ground-state conformations are represented by crystal-structure geometries.

6.2. Speculated implications of 611N–601N dimer results

While not ‘on-pathway’ with respect to energy transfer between two intrinsic Car/Chl states, we speculate that ‘off-pathway’ coupling—that is, coupling outside of the $\{S_1, S_2, Q_x, Q_y\}$ four-state basis—between these S_2 locally excited (1 LE) and 1 CT states may manifest. This manifestation would stem from non-adiabatic, or vibronic, dynamics based on time-dependent overlaps between states of LE and CT character. We remark that S_2 -CT population transfer relaxes the symmetry selection rules that otherwise limit the vibrational-mode symmetries facilitating S_2 population transfer to S_1 . This may help explain the observation of sub-200-fs Chl- a ground-state bleaching within the S_2 depopulation window (50–300 fs) [3,27].

What might be the fate of this CT state if it were to be populated? The exceptionally small transition dipole moment of this state suggests a negligible exchange energy separating 1 CT from 3 CT, where 3 CT is the corresponding charge-transfer state of triplet spin multiplicity. Thus, while our calculation of a lower-lying Chl- a Q_y singlet state leads us to speculate that 1 CT might internally convert to Q_y once populated, we also speculate that this off-pathway dark multichromophoric

state might lead to intersystem crossing into the triplet manifold. The second-order spin–vibronic coupling [53–55] mechanism, whereby vibronic coupling mediates transfer between CT states of different multiplicity through 1 LE states, is likely to drive the intersystem crossing, given that direct spin–orbit coupling between such CT states is forbidden by El-Sayed’s rules [56,57]. This is why we label two possible fates for the CT state in figure 3: internal conversion and intersystem crossing. We note that experimentalists also have speculated on a ‘delocalized triplet state’ connecting Car and Chl- a in PCP [58], and we suggest that such a state may be CT in origin. This would supply an additional photoprotective mechanism for Cars in PCP [58] and thus hint at the CT state’s purpose.

6.3. The Car–Car 611N–612N dimer

Let us now turn our attention to the other computed dark multichromophoric state: what we label as the S^* state appearing for the Car dimer system. Our S^* label is based on the literature assignment of a dark state appearing only in photosynthetic antenna complexes—that is, a state that is not intrinsic to independent chromophores—and potentially playing a role in the singlet-fission mechanism of ultrafast triplet-state generation [11,59–62] (‘fission’, figure 3). Singlet fission leads to ultrafast triplet-state generation due to the population of a correlated triplet pair intermediate singlet state following one-photon photoexcitation—making the triplet-generation process spin-allowed [63].

Here, we remark that the S^* wave function we compute for the Car dimer (table 4 and figure 3) appears to be such an intermediate. This is suggested by $E(S^*) \cong E(T_1) + E(T_2)$ and the pure four-unpaired-electron nature of this state that we glean quantitatively by computing N_{odd} (table 4). As indicated in table 4, the N_{odd} value of S^* not only equals the ideal value for a correlated triplet pair of spatially decoupled spin-paired triplet excitations, but also is 0.79 greater than the N_{odd} value of the intrinsic Car S_1 state. While singlet-excitation contamination of S_1 is expected to hinder the intramolecular-singlet-fission process, we remark that S^* may unlock the intermolecular-singlet-fission process observed in carotenoid aggregates [44,64]. Further evidence of S^* fissionability is found in the quasidegeneracy between S^* and the lowest-lying quintet state of the Car dimer—indicating a negligible exchange splitting and an effectively non-interacting pair of spin-paired triplets. Finally, we note that this correlated triplet pair is predominantly characterized by two superimposed charge-transfer excitations between the Cars, which not only explains its exceptionally small transition dipole moment (table 4), but also indicates how superexchange could couple S^* (1 TT) to S_2 (1 LE) *via* the CT state according to the second-order electronic coupling formulation involving states with charge-transfer character [65].

That competitive population of this correlated triplet pair in lieu of internal conversion to S_1 could elicit singlet fission was also articulated by Musser *et al.* [44], though they did not adopt the S^* label we use here. We note that carotenoids are aggregated natively in photosynthetic antenna complexes such as PCP, and because correlated triplet pairs have been described as dimer-pair-specific [66–68], we simulate the intermolecular correlated triplet pair in aggregates simply by using the crystal-structure nearest-neighbour Car–Car dimer-pair orientation. Our results help to validate the arguments in

Musser *et al.* [44] that through-space interactions between carotenoids manifest in a fissionable correlated triplet pair.

6.4. Speculated implications of 611N–612N dimer results

Nonetheless, there exists an important caveat. For Musser *et al.* [44] to have observed sub-100-fs ultrafast singlet fission as they report, the correlated triplet pair must have been *strongly* coupled to the photoexcited state to outcompete S_2 – S_1 internal conversion kinetically. On the other hand, we surmise that our correlated triplet pair S^* state would be *weakly* coupled to the photoexcited state because of the weakly overlapping superposition nature of the two-particle transition, meaning that the consequential lack of charge-transfer/triplet-pair mixing [65] would lead to weak second-order superexchange-based coupling.

In fact, we speculate that this weak CT-based coupling to the S^* state allows for the observed energy-transfer efficiency in PCP to be so exceptional [3]. We reiterate that the S^* dark multichromophoric state represents an *off-pathway* intermediate in the context of energy transfer to Chl-*a*, since its population corresponds to activation of the singlet-fission mechanism that populates low-lying Car triplets in lieu of transferring excitation energy to the Chl-*a* Q_x and Q_y singlet states [11]. While we compute that S^* population from S_2 is *thermodynamically* favourable, its *kinetic* competitiveness with S_2 – S_1 internal conversion is doubtful in light of the 6.84 Å intermolecular separation.

That improving fissionability of the correlated triplet pair leads to worsening the kinetic competitiveness of its population is a problem that has been thoroughly analysed by Pensack *et al.* [69] and described as ‘striking the right balance of intermolecular coupling for high-efficiency singlet fission.’ Essentially, for intermolecular singlet fission to achieve optimal efficiency, the spatial overlap must be decreased only to the extent that correlated triplet pair formation can remain kinetically competitive with populating trap states (such as the Car S_1 state). The purity of the Car–Car dimer ^1TT state hints that this limit has been exceeded, enabling the energy-transfer pathways like S_1 – Q_y (see ‘ S_1 Emission’ in table 4 and figure 3) to dominate. We briefly remark that the S_1 emission and Q_y absorption energies underlying this pathway are in agreement with experimental values [26] and would seem to support the notion of energy transfer from the impure dark correlated triplet pair S_1 state with non-negligible oscillator strength. Yet we speculate that Car–Car intermolecular coupling can be tuned by protein breathing motions under conditions of excessive photon flux so as to activate the photoprotective mechanism and disrupt this energy-transfer pathway [4]. We thus comment that this report may serve as the basis for future quantum dynamical investigations involving these multichromophoric systems—embedded in the native protein environment—to investigate further what we surmise here.

7. Conclusion

In this report, we have evaluated the intrinsic and multichromophoric manifolds of peridinin Car and Chl-*a* excited states in their native PCP environments and conformations so as to understand how nature’s complexity controls photophysical properties. We find that the native interchromophore orientations in PCP clusters support dark multichromophoric

excited states sustained by through-space electrostatic interactions between adjacent pigments. In addition to identifying the S_1 and S_2 lowest-lying Car bright/dark states, as well as the Q_y and Q_x lowest-lying Chl-*a* bright/dark states, we uncover two additional states that are not intrinsic to Car or Chl. We label these states as S^* and CT in accordance with their wave function properties: S^* is computed to be a fissionable correlated triplet pair, while CT is computed to be a long-range charge-transfer state between a Chl HOMO and neighbouring Car LUMO. We speculate that S^* and CT account for two photophysical phenomena determined experimentally: singlet fission in carotenoid aggregates and sub-200-fs Chl-*a* bleaching in PCP, respectively. We also note that these states may serve to funnel population toward triplet-state formation in lieu of singlet energy transfer.

8. Computational details

PCP geometrically was extracted from its *A. carterae* crystal structure (PDB ID 1PPR) [26,70] and adapted to include only residues associated with subunit N. Hydrogen atoms were added to these residues using *GaussView* (v. 6.0.16). Following the correct application of hydrogen atoms to residue 611N—corresponding to the carotenoid peridinin—to form the correct peridinin chemical formula ($C_{39}H_{50}O_7$), the resulting atomic coordinates were extracted from PCP and used for the single-molecule excited-state electronic-structure calculations yielding the results in table 1 and figure 1. These excited-state electronic-structure calculations were carried out using state-specific NEVPT2 on top of state-averaged CASSCF and DMRGSCF wave functions using algorithms launched through *PySCF* [71] that, in the case of DMRGSCF, was interfaced with the *BLOCK* [72–76] algorithm (v. 1.1.1).

We have detailed our application of CASSCF/DMRGSCF and NEVPT2 in prior publications [45,47,48]. Briefly, we considered the variational quality of the wave functions computed across different active spaces by comparing variational CAS/DMRGSCF excitation energies with those after applying NEVPT2. Starting with active spaces correlating the two highest-energy occupied (along with their four total electrons) and two lowest-energy unoccupied orbitals in the mean-field picture (4,4), we expanded this active space up to a complete- π -orbital-active space (16,16). In the process, we incorporated progressively higher-lying excited states into our state averaging with predominant configurations corresponding to lower-lying and higher-lying molecular orbitals.

We assessed these predominant configurations by looking at CASSCF wave function configuration coefficients and DMRGSCF one- and two-particle transition densities. We noticed that the smallest discrepancy between variational and perturbative excitation energies was obtained for the bright S_2 state (dynamically correlated) using the (4,4) active space, whereas that for the non-dynamically correlated dark states was obtained using the complete- π (16,16) active space. We obtained transition dipole moments and odd-electron counts using the one-particle transition and reduced density matrices, respectively, for these wave functions. These methods formed the basis for our crystal-structure results in table 1 and figure 1.

We then considered geometry optimizations of peridinin 611N in its native PCP environment using the QM/MM approach carried out with the *ONIOM* [77–87] keyword in

Gaussian 16 [88]. We optimized the bright S_2 excited-state geometry using the single-reference Tamm–Dancoff approximation (TDA) to time-dependent density functional theory—applying the Def2SVP basis set and PBE1PBE functional for the QM layer containing 611N and the universal force field (UFF) for the MM layer containing all other residues—via an ONIOM calculation with *Gaussian 16* [88]. These other residues included the three Car and one Chl molecules in the chromophore cluster containing 611N, as well as all amino acids and the two DGD molecules associated with subunit N according to its crystal structure. As the objective in this work was to consider the impact of the PCP protein scaffold on peridinin reorganization and interaction with other pigments, we eliminated all water residues associated with subunit N so as to make the calculation independent of solvent.

We applied the same truncated PCP crystal environment to an excited-state geometry optimization calculation of the S_1 state—this time using CASSCF with the Def2SVP basis set and a four-orbital, four-electron active space (4,4) as the QM level to capture this dark-state wave function. We extracted the 611N S_2 and S_1 geometries yielded by these calculations for subsequent single-molecule 611N excited-state wave function and energy analysis using multireference perturbation theory, leading to the results in table 3/figure 2 and table 4/figure 3, respectively. All calculations in the tables and figures of this manuscript were based on pure QM calculations without consideration of the surrounding PCP environment, which was considered only for the geometry optimizations and crystal-structure chromophore orientations. We expanded the number of states and active space in the same manner as before.

For the multichromophoric calculations leading to the results in table 4/figure 3, we computed the change in the manifold of excited states for 611N in a collective quantum system encompassing 612N to form a QM 611N–612N Car dimer pair, as well as the change in the manifold of excited states for 611N in a collective quantum system encompassing 601N to form a QM 611N–601N Car–Chl dimer pair. We did not attempt calculations on the 611N–612N–601N trimer system, but we

instead considered the interactions between 611N and 601N, as well as 611N and 612N, in separate calculations.

For the Car–Car dimer pair, we first performed a three-state-averaged CASSCF(4,4) calculation to optimize the ground state together with the lowest-lying singlet and quintet correlated triplet pair states. We then used these multireference optimized orbitals as the initial guess for a subsequent spin-state-averaged calculation using spin-adapted DMRGSCF(8,8) encompassing five singlets, five triplets and one quintet.

For the Car–Chl dimer pair, we first performed a five-singlet-state-averaged DMRGSCF(8,8) calculation to acquire multireference optimized orbitals that were used as the initial guess for a subsequent six-singlet-state-averaged DMRGSCF(16,16) calculation. We identified the excited states listed in table 4 by considering their largest one- and two-particle transition density matrix elements corresponding to optimized multireference molecular orbitals that we found to be single-molecule-specific based on their visualization using *Jmol* [89] from *Molden* [90] files printed using *PySCF*. The S_1 absorption energy listed in table 4 was computed from the Car–Car dimer system, and all multireference perturbation theory calculations in this manuscript were performed with the cc-pVDZ basis set.

Data accessibility. Supplementary files available as part of the electronic supplementary material.

Authors' contributions. E.J.T. designed the project/manuscript and carried out the calculations. F.F. contributed to the theoretical analysis of the computation and provided organizational support for the manuscript. Z.S.D.T. performed an additional geometric analysis of Peridinin–Chlorophyll–Protein. D.B. contributed to the theoretical analysis of the computation and provided editorial support for the manuscript. G.D.S. contributed to the theoretical analysis of the computation and provided final editorial support for the manuscript.

Competing interests. We declare we have no competing interests.

Funding. E.J.T. was funded by a Belgian American Educational Foundation research fellowship.

Acknowledgements. This work is generously funded by the Bioinspired Light-Escalated Chemistry Energy Frontier Research Centre funded by the U.S. Department of Energy, Office of Science, Office of Basic Energy Sciences, under Award DE-SC0019370. F.F. acknowledges financial support from the European Union's H2020 Marie Skłodowska-Curie actions, grant no. 799408.

References

- Frank HA, Cogdell RJ. 1996 Carotenoids in photosynthesis. *Photochem. Photobiol.* **63**, 257–264. (doi:10.1111/j.1751-1097.1996.tb03022.x)
- Scholes GD. 2010 Quantum-coherent electronic energy transfer: did nature think of it first? *J. Phys. Chem. Lett.* **1**, 2–8. (doi:10.1021/jz900062f)
- Zigmantas D, Hiller RG, Sundström V, Polívka T. 2002 Carotenoid to chlorophyll energy transfer in the peridinin–chlorophyll–a–protein complex involves an intramolecular charge transfer state. *Proc. Natl Acad. Sci. USA* **99**, 16 760–16 765. (doi:10.1073/pnas.262537599)
- Hashimoto H, Uragami C, Yukihira N, Gardiner AT, Cogdell RJ. 2018 Understanding/unravelling carotenoid excited singlet states. *J. R. Soc. Interface* **15**, 20180026. (doi:10.1098/rsif.2018.0026)
- Hofmann E, Wrench PM, Sharples FP, Hiller RG, Welte W, Diederichs K. 1996 Structural basis of light harvesting by carotenoids: peridinin–chlorophyll–protein from *Amphidinium carterae*. *Science* **272**, 1788–1791. (doi:10.1126/science.272.5269.1788)
- Reimers JR, Cai Z-L, Kobayashi R, Ratsep M, Freiberg A, Krausz E. 2013 Assignment of the Q-bands of the chlorophylls: coherence loss via Q_x – Q_y mixing. *Sci. Rep.* **3**, 2761. (doi:10.1038/srep02761)
- Hudson BS, Kohler BE. 1972 A low-lying weak transition in the polyene α,ω -diphenyloctatetraene. *Chem. Phys. Lett.* **14**, 299–304. (doi:10.1016/0009-2614(72)80119-2)
- Hudson BS, Kohler BE, Schulten K. 1982 Linear polyene electronic structure and potential surfaces. In *Excited states* (ed. EC Lim), pp. 1–95. Amsterdam, The Netherlands: Elsevier.
- Kohler BE, Spangler C, Westerfield C. 1988 The 2^1A_g state in the linear polyene 2,4,6,8,10,12,14,16-octadecaoctaene. *J. Chem. Phys.* **89**, 5422–5428. (doi:10.1063/1.455594)
- Cerullo G, Polli D, Lanzani G, De Silvestri S, Hashimoto H, Cogdell RJ. 2002 Photosynthetic light harvesting by carotenoids: detection of an intermediate excited state. *Science* **298**, 2395–2398. (doi:10.1126/science.1074685)
- Polívka T, Sundström V. 2009 Dark excited states of carotenoids: consensus and controversy. *Chem. Phys. Lett.* **477**, 1–11. (doi:10.1016/j.cplett.2009.06.011)
- Gouterman M, Stryer L. 1962 Fluorescence polarization of some porphyrins. *J. Chem. Phys.* **37**, 2260–2266. (doi:10.1063/1.1732996)
- Gouterman M. 1961 Spectra of porphyrins. *J. Mol. Spectrosc.* **6**, 138–163. (doi:10.1016/0022-2852(61)90236-3)
- Weiss C. 1972 The π electron structure and absorption spectra of chlorophylls in solution. *J. Mol. Spectrosc.* **44**, 37–80. (doi:10.1016/0022-2852(72)90192-0)

15. Fragata M, Nördén B, Kurcsev T. 1988 Linear dichroism of chlorophyll-*a* and pheophytin *a* oriented in a lamellar phase of glycerylmonooctanoate/H₂O: characterization of electronic transitions. *Photochem. Photobiol.* **47**, 133–143. (doi:10.1111/j.1751-1097.1988.tb02703.x)
16. Umetsu M, Wang Z-Y, Kobayashi M, Nozawa T. 1999 Interaction of photosynthetic pigments with various organic solvents: magnetic circular dichroism approach and application to chlorosomes. *Biochim. Biophys. Acta* **1410**, 19–31. (doi:10.1016/S0005-2728(98)00170-4)
17. Umetsu M, Wang Z-Y, Yoza K, Kobayashi M, Nozawa T. 2000 Interaction of photosynthetic pigments with various organic solvents 2: application of magnetic circular dichroism to bacteriochlorophyll *a* and light-harvesting complex1. *Biochim. Biophys. Acta* **1457**, 106–117. (doi:10.1016/S0005-2728(00)00070-0)
18. Macpherson AN, Gillbro T. 1998 Solvent dependence of the ultrafast S₂–S₁ internal conversion rate of β-carotene. *J. Phys. Chem. A* **102**, 5049–5058. (doi:10.1021/jp980979z)
19. Förster T, Sinanoglu O. 1965 *Modern quantum chemistry*, vol. 3, New York, NY: Academic Press.
20. Bautista JA, Connors RE, Raju BB, Hiller RG, Sharples FP, Gosztola D, Wasielewski MR, Frank HA. 1999 Excited state properties of peridinin: observation of a solvent dependence of the lowest excited singlet state lifetime and spectral behavior unique among carotenoids. *J. Phys. Chem. B* **103**, 8751–8758. (doi:10.1021/jp9916135)
21. Beck WF, Bishop MM, Roscioli JD, Ghosh S, Frank HA. 2015 Excited state conformational dynamics in carotenoids: dark intermediates and excitation energy transfer. *Arch. Biochem. Biophys.* **572**, 175–183. (doi:10.1016/j.abb.2015.02.016)
22. Ghosh S, Bishop MM, Roscioli JD, LaFountain AM, Frank HA, Beck WF. 2016 Femtosecond heterodyne transient grating studies of nonradiative deactivation of the S₂ (1¹B_u⁺) state of peridinin: detection and spectroscopic assignment of an intermediate in the decay pathway. *J. Phys. Chem. B* **120**, 3601–3614. (doi:10.1021/acs.jpcc.5b12753)
23. Ghosh S, Roscioli JD, Bishop MM, Gurchiek JK, LaFountain AM, Frank HA, Beck WF. 2016 Torsional dynamics and intramolecular charge transfer in the S₂ (1¹B_u⁺) excited state of peridinin: a mechanism for enhanced mid-visible light harvesting. *J. Phys. Chem. Lett.* **7**, 3621–3626. (doi:10.1021/acs.jpcclett.6b01642)
24. Vaswani HM, Hsu C-P, Head-Gordon M, Fleming GR. 2003 Quantum chemical evidence for an intramolecular charge-transfer state in the carotenoid peridinin of peridinin–chlorophyll–protein. *J. Phys. Chem. B* **107**, 7940–7946. (doi:10.1021/jp030086t)
25. Knecht S, Marian CM, Kongsted J, Mennucci B. 2013 On the photophysics of carotenoids: a multireference DFT study of peridinin. *J. Phys. Chem. B* **117**, 13 808–13 815. (doi:10.1021/jp4078739)
26. Bricker WP, Lo CS. 2014 Excitation energy transfer in the peridinin–chlorophyll *a*–protein complex modeled using configuration interaction. *J. Phys. Chem. B* **118**, 9141–9154. (doi:10.1021/jp5017054)
27. Bricker WP, Lo CS. 2015 Efficient pathways of excitation energy transfer from delocalized S₂ excitons in the peridinin–chlorophyll *a*–protein complex. *J. Phys. Chem. B* **119**, 5755–5764. (doi:10.1021/jp511766j)
28. Krueger BP, Lampoura SS, van Stokkum IHM, Papagiannakis E, Salverda JM, Gradinaru CC, Rutkauskas D, Hiller RG, van Grondelle R. 2001 Energy transfer in the peridinin chlorophyll-*a* protein of *Amphidinium carterae* studied by polarized transient absorption and target analysis. *Biophys. J.* **80**, 2843–2855. (doi:10.1016/S0006-3495(01)76251-0)
29. Fassioi F, Dinshaw R, Arpin PC, Scholes GD. 2014 Photosynthetic light harvesting: excitons and coherence. *J. R. Soc. Interface* **11**, 20130901. (doi:10.1098/rsif.2013.0901)
30. Scholes GD, Fleming GR. 2000 On the mechanism of light harvesting in photosynthetic purple bacteria: B800 to B850 energy transfer. *J. Phys. Chem. B* **104**, 1854–1868. (doi:10.1021/jp9934351)
31. Sisto A *et al.* 2017 Atomistic non-adiabatic dynamics of the LH2 complex with a GPU-accelerated ab initio exciton model. *Phys. Chem. Chem. Phys.* **19**, 14 924–14 936. (doi:10.1039/C7CP00492C)
32. Huelga SF, Plenio MB. 2014 Quantum biology: a vibrant environment. *Nat. Phys.* **10**, 621–622. (doi:10.1038/nphys3047)
33. Ishizaki A, Fleming GR. 2011 On the interpretation of quantum coherent beats observed in two-dimensional electronic spectra of photosynthetic light harvesting complexes. *J. Phys. Chem. B* **115**, 6227–6233. (doi:10.1021/jp112406h)
34. Engel GS, Calhoun TR, Read EL, Ahn T-K, Mančal T, Cheng Y-C, Blankenship RE, Fleming GR. 2007 Evidence for wavelike energy transfer through quantum coherence in photosynthetic systems. *Nature* **446**, 782–786. (doi:10.1038/nature05678)
35. Lee H, Cheng Y-C, Fleming GR. 2007 Coherence dynamics in photosynthesis: protein protection of excitonic coherence. *Science* **316**, 1462–1465. (doi:10.1126/science.1142188)
36. Collini E, Wong CY, Wilk KE, Curmi PMG, Brumer P, Scholes GD. 2010 Coherently wired light-harvesting in photosynthetic marine algae at ambient temperature. *Nature* **463**, 644–647. (doi:10.1038/nature08811)
37. Panitchayangkoon G, Voronine DV, Abramavicius D, Caram JR, Lewis NHC, Mukamel S, Engel GS. 2011 Direct evidence of quantum transport in photosynthetic light-harvesting complexes. *Proc. Natl Acad. Sci. USA* **108**, 20 908–20 912. (doi:10.1073/pnas.1105234108)
38. Scholes GD. 2011 Quantum biology: coherence in photosynthesis. *Nat. Phys.* **7**, 448–449. (doi:10.1038/nphys2013)
39. Chenu A, Scholes GD. 2015 Coherence in energy transfer and photosynthesis. *Annu. Rev. Phys. Chem.* **66**, 69–96. (doi:10.1146/annurev-physchem-040214-121713)
40. Wong CY, Alvey RM, Turner DB, Wilk KE, Bryant DA, Curmi PMG, Silbey RJ, Scholes GD. 2012 Electronic coherence lineshapes reveal hidden excitonic correlations in photosynthetic light harvesting. *Nat. Chem.* **4**, 396–404. (doi:10.1038/nchem.1302)
41. Brédas J-L, Sargent EH, Scholes GD. 2017 Photovoltaic concepts inspired by coherence effects in photosynthetic systems. *Nat. Mater.* **16**, 35–44. (doi:10.1038/nmat4767)
42. Scholes GD *et al.* 2017 Using coherence to enhance function in chemical and biophysical systems. *Nature* **543**, 647–656. (doi:10.1038/nature21425)
43. Scholes GD, Fleming GR, Olaya-Castro A, van Grondelle R. 2011 Lessons from nature about solar light harvesting. *Nat. Chem.* **3**, 763–774. (doi:10.1038/nchem.1145)
44. Musser AJ, Mairuri M, Brida D, Cerullo G, Friend RH, Clark J. 2015 The nature of singlet exciton fission in carotenoid aggregates. *J. Am. Chem. Soc.* **137**, 5130–5139. (doi:10.1021/jacs.5b01130)
45. Taffet EJ, Scholes GD. 2018 Peridinin torsional distortion and bond-length alternation introduce intramolecular charge-transfer and correlated triplet pair intermediate excited states. *J. Phys. Chem. B* **122**, 5835–5844. (doi:10.1021/acs.jpcc.8b02504)
46. Liebel M, Schnedermann C, Kukura P. 2014 Vibrationally coherent crossing and coupling of electronic states during internal conversion in β-Carotene. *Phys. Rev. Lett.* **112**, 198302. (doi:10.1103/PhysRevLett.112.198302)
47. Taffet EJ, Scholes GD. 2017 The A_g⁺ state falls below 3A_g⁻ at carotenoid-relevant conjugation lengths. *Chem. Phys.* **515**, 757–767. (doi:10.1016/j.chemphys.2017.12.008)
48. Taffet EJ, Olivier Y, Lam F, Beljonne D, Scholes GD. 2018 Carbene–metal–amide bond deformation, rather than ligand rotation, drives delayed fluorescence. *J. Phys. Chem. Lett.* **9**, 1620–1626. (doi:10.1021/acs.jpcclett.8b00503)
49. Tavan P, Schulten K. 1986 The low-lying electronic excitations in long polyenes: a PPP-MRD-CI study. *J. Chem. Phys.* **85**, 6602–6609. (doi:10.1063/1.451442)
50. Polívka T, Sundström V. 2004 Ultrafast dynamics of carotenoid excited states—from solution to natural and artificial systems. *Chem. Rev.* **104**, 2021–2072. (doi:10.1021/cr020674n)
51. Feng X, Luzanov AV, Krylov AI. 2013 Fission of entangled spins: an electronic structure perspective. *J. Phys. Chem. Lett.* **4**, 3845–3852. (doi:10.1021/jz402122m)
52. Linnanto J, Korppi-Tommola J. 2006 Quantum chemical simulation of excited states of chlorophylls, bacteriochlorophylls and their complexes. *Phys. Chem. Chem. Phys.* **8**, 663–687. (doi:10.1039/B513086G)
53. Penfold TJ, Gindensperger E, Daniel C, Marian CM. 2018 Spin–vibronic mechanism for intersystem crossing. *Chem. Rev.* **118**, 6975–7025. (doi:10.1021/acs.chemrev.7b00617)
54. Etherington MK, Gibson J, Higginbotham HF, Penfold TJ, Monkman AP. 2016 Revealing the spin–vibronic coupling mechanism of thermally activated

- delayed fluorescence. *Nat. Commun.* **7**, 13680. (doi:10.1038/ncomms13680)
55. Gibson J, Monkman AP, Penfold TJ. 2016 The importance of vibronic coupling for efficient reverse intersystem crossing in thermally activated delayed fluorescence molecules. *Chem. Phys. Chem.* **17**, 2956–2961. (doi:10.1002/cphc.201600662)
 56. Li EY-T, Jiang T-Y, Chi Y, Chou P-T. 2014 Semi-quantitative assessment of the intersystem crossing rate: an extension of the El-Sayed rule to the emissive transition metal complexes. *Phys. Chem. Chem. Phys.* **16**, 26 184–26 192. (doi:10.1039/C4CP03540B)
 57. El-Sayed MA. 1963 Spin-orbit coupling and the radiationless processes in nitrogen heterocyclics. *J. Chem. Phys.* **38**, 2834–2838. (doi:10.1063/1.1733610)
 58. Alexandre MTA, Lührs DC, van Stokkum IHM, Hiller R, Groot M-L, Kennis JTM, van Grondelle R. 2007 Triplet state dynamics in peridinin–chlorophyll-a–protein: a new pathway of photoprotection in LHCs? *Biophys. J.* **93**, 2118–2128. (doi:10.1529/biophysj.107.106674)
 59. Gradinaru CC, Kennis JTM, Papagiannakis E, van Stokkum IHM, Cogdell RJ, Fleming GR, Niederman RA, van Grondelle R. 2001 An unusual pathway of excitation energy deactivation in carotenoids: singlet-to-triplet conversion on an ultrafast timescale in a photosynthetic antenna. *Proc. Natl Acad. Sci. USA*, **98**, 2364–2369. (doi:10.1073/pnas.051501298)
 60. Papagiannakis E, Kennis JTM, van Stokkum IHM, Cogdell RJ, van Grondelle R. 2002 An alternative carotenoid-to-bacteriochlorophyll energy transfer pathway in photosynthetic light harvesting. *Proc. Natl Acad. Sci. USA* **99**, 6017–6022. (doi:10.1073/pnas.092626599)
 61. Papagiannakis E, Das SK, Gall A, van Stokkum IHM, Robert B, van Grondelle R, Frank HA, Kennis JTM. 2003 Light harvesting by carotenoids incorporated into the B850 light-harvesting complex from rhodospira rubra: excited-state relaxation, ultrafast triplet formation, and energy transfer to bacteriochlorophyll. *J. Phys. Chem. B* **107**, 5642–5649. (doi:10.1021/jp027174i)
 62. Ostroumov EE, Reus MGMM, Holzwarth AR. 2011 On the nature of the ‘dark S^{*}’ excited state of β -carotene. *J. Phys. Chem. A* **115**, 3698–3712. (doi:10.1021/jp105385c)
 63. Sanders SN *et al.* 2015 Quantitative intramolecular singlet fission in bipentacenes. *J. Am. Chem. Soc.* **137**, 8965–8972. (doi:10.1021/jacs.5b04986)
 64. Wang C, Tauber MJ. 2010 High-yield singlet fission in a zeaxanthin aggregate observed by picosecond resonance raman spectroscopy. *J. Am. Chem. Soc.* **132**, 13 988–13 991. (doi:10.1021/ja102851m)
 65. Berkelbach TC, Hybertsen MS, Reichman DR. 2013 Microscopic theory of singlet exciton fission. II. Application to pentacene dimers and the role of superexchange. *J. Chem. Phys.* **138**, 114103. (doi:10.1063/1.4794427)
 66. Bayliss SL, Weiss LR, Rao A, Friend RH, Chepelianski AD, Greenham NC. 2016 Spin signatures of exchange-coupled triplet pairs formed by singlet fission. *Phys. Rev. B* **94**, 045204. (doi:10.1103/PhysRevB.94.045204)
 67. Weiss LR *et al.* 2017 Strongly exchange-coupled triplet pairs in an organic semiconductor. *Nat. Phys.* **13**, 176–181. (doi:10.1038/NPHYS3908)
 68. Bayliss SL *et al.* 2018 Site-selective measurement of coupled spin pairs in an organic semiconductor. *Proc. Natl Acad. Sci. USA* **115**, 5077–5082. (doi:10.1073/pnas.1718868115)
 69. Pensack RD *et al.* 2018 Striking the right balance of intermolecular coupling for high-efficiency singlet fission. *Chem. Sci.* **9**, 6240–6259. (doi:10.1039/C8SC00293B)
 70. Berman HM, Westbrook J, Feng Z, Gilliland G, Bhat TN, Weissig H, Shindyalov IN, Bourne PE. 2000 The protein data bank. *Nucleic Acids Res.* **28**, 235–242. (doi:10.1093/nar/28.1.235)
 71. Sun Q *et al.* 2018 PySCF: the python-based simulations of chemistry framework. *WIREs Comput. Mol. Sci.* **8**, e1340. (doi:10.1002/wcms.1340)
 72. Chan GK-L, Head-Gordon M. 2002 Highly correlated calculations with a polynomial cost algorithm: a study of the density matrix renormalization group. *J. Chem. Phys.* **116**, 4462–4476. (doi:10.1063/1.1449459)
 73. Chan GK-L. 2004 An algorithm for large scale density matrix renormalization group calculations. *J. Chem. Phys.* **120**, 3172–3178. (doi:10.1063/1.1638734)
 74. Ghosh D, Hachmann J, Yanai T, Chan GK-L. 2008 Orbital optimization in the density matrix renormalization group, with applications to polyenes and β -carotene. *J. Chem. Phys.* **128**, 144117. (doi:10.1063/1.2883976)
 75. Sharma S, Chan GK-L. 2012 Spin-adapted density matrix renormalization group algorithms for quantum chemistry. *J. Chem. Phys.* **136**, 124121. (doi:10.1063/1.3695642)
 76. Guo S, Watson MA, Hu W, Sun Q, Chan GK-L. 2016 N-electron valence state perturbation theory based on a density matrix renormalization group reference function, with applications to the chromium dimer and a trimer model of poly(p-phenylenevinylene). *J. Chem. Theory Comput.* **12**, 1583–1591. (doi:10.1021/acs.jctc.5b01225)
 77. Dapprich S, Komáromi I, Byun KS, Morokuma K, Frisch MJ. 1999 A new ONIOM implementation in Gaussian98. Part I. The calculation of energies, gradients, vibrational frequencies and electric field derivatives. *J. Mol. Struct.: THEOCHEM* **461–462**, 1–21. (doi:10.1016/S0166-1280(98)00475-8)
 78. Vreven T, Byun KS, Komáromi I, Dapprich S, Montgomery JA, Morokuma K, Frisch MJ. 2006 Combining quantum mechanics methods with molecular mechanics methods in ONIOM. *J. Chem. Theory Comput.* **2**, 815–826. (doi:10.1021/ct050289g)
 79. Vreven T, Morokuma K. 2006 Chapter 3 hybrid methods: ONIOM(QM:MM) and QM/MM. In *Annual reports in computational chemistry* (ed. DC Spellmeyer), pp. 35–51. Amsterdam, The Netherlands: Elsevier.
 80. Clemente FR, Vreven T, Frisch MJ. 2010 Getting the most out of ONIOM: guidelines and pitfalls. In *Quantum biochemistry*, pp. 61–83. Hoboken, NJ: John Wiley & Sons, Ltd.
 81. Orozco M *et al.* 2007 Beyond the continuum approach. In *Continuum solvation models in chemical physics*, pp. 499–605. Hoboken, NJ: John Wiley & Sons, Ltd.
 82. Maseras F, Morokuma K. 1995 IMOMM: a new integrated ab initio + molecular mechanics geometry optimization scheme of equilibrium structures and transition states. *J. Comput. Chem.* **16**, 1170–1179. (doi:10.1002/jcc.540160911)
 83. Humbel S, Sieber S, Morokuma K. 1996 The IMOMO method. Integration of different levels of molecular orbital approximations for geometry optimization of large systems. Test for n-butane conformation and SN2 reaction: RCl^+Cl^- . *J. Chem. Phys.* **105**, 1959–1967. (doi:10.1063/1.472065)
 84. Matsubara T, Sieber S, Morokuma K. 1996 A test of the new ‘integrated MO + MM’ (IMOMM) method for the conformational energy of ethane and n-butane. *Int. J. Quantum Chem.* **60**, 1101–1109. (doi:10.1002/(SICI)1097-461X(1996)60:6<1101::AID-QUA1>3.0.CO;2-3)
 85. Svensson M, Humbel S, Froese RDJ, Matsubara T, Sieber S, Morokuma K. 1996 ONIOM: a multilayered integrated MO + MM method for geometry optimizations and single point energy predictions. A test for diels–alder reactions and Pt(P(t-Bu)₃)₂ + H₂ oxidative addition. *J. Phys. Chem.* **100**, 19 357–19 363. (doi:10.1021/jp962071j)
 86. Svensson M, Humbel S, Morokuma K. 1996 Energetics using the single point IMOMO (integrated molecular orbital + molecular orbital) calculations: choices of computational levels and model system. *J. Chem. Phys.* **105**, 3654–3661. (doi:10.1063/1.472235)
 87. Vreven T, Morokuma K. 2000 On the application of the IMOMO (integrated molecular orbital + molecular orbital) method. *J. Comput. Chem.* **21**, 1419–1432. (doi:10.1002/1096-987X(200012)21:16<1419::AID-JCC1>3.0.CO;2-C)
 88. Frisch MJ *et al.* 2016 *Gaussian 16*. Gaussian, Inc.: Wallingford, CT.
 89. Hanson RM. 2010 Jmol – a paradigm shift in crystallographic visualization. *J. Appl. Cryst.* **43**, 1250–1260. (doi:10.1107/S0021889810030256)
 90. Schaffenaar G, Noordik JH. 2000 Molden: a pre- and post-processing program for molecular and electronic structures. *J. Comput.-Aided Mol. Des.* **14**, 123–134. (doi:10.1023/a:1008193805436)